III Science, Technology and Innovation Fair of UFSM-CS

Analysis of a Thermoelectric Air Dehumidifier

Análise de um Desumidificador Termoelétrico

Mathias Verdum de Almeida[I] iD, **Arthur Sandri Lunkes**[I] iD,
Juan Augusto Mayer Copetti[I] iD, **Matheus Fritz Warol Porto Rodrigues**[I] iD,
Maximiliano Silveira de Souza[I] iD, **Cristiano Frandalozo Maidana**[I] iD,
Charles Rech[I] iD, **André Francisco Caldeira**[I] iD, **Simone Ferigolo Venturini**[I] iD,
Carmen Brum Rosa[I] iD

[I] Universidade Federal de Santa Maria, Cachoeira do Sul, RS, Brasil

ABSTRACT

The present study aims to analyze a thermoelectric air dehumidifier. To this end, knowledge of transport phenomena was applied in combination with experimental measurements of temperature at the heat sinks and the mass flow rate of extracted water. A mathematical model was developed based on an air dehumidifier equipped with a Peltier module, showing a deviation of 16.3% from the experimentally determined water production. The developed model indicates that the device does not operate with an adequate volumetric airflow to achieve maximum efficiency. This highlights the need for future studies in which the proposed improvements are implemented and the device is re-evaluated.

Keywords: Dehumidifier; Thermoelectric; Peltier

RESUMO

O presente estudo tem como objetivo realizar a análise de um desumidificador de ar termoelétrico. Para isso, foram utilizados conhecimentos sobre os fenômenos de transporte, combinados com a realização de medições experimentais de temperatura nos dissipadores de calor e vazão mássica de extração de água. Desse modo, um modelo matemático baseado em um desumidificador de ar equipado com uma pastilha Peltier foi desenvolvido, apresentando uma divergência de 16,3% em relação à produção de água determinada experimentalmente. Através do modelo desenvolvido, é possível inferir que o dispositivo utilizado não possui uma vazão volumétrica de ar adequada para sua máxima eficiência. Ressalta-se a necessidade de realização de trabalhos futuros em que as melhorias elencadas sejam implementadas e o dispositivo reavaliado.

Palavras-chave: Desumidificador; Termoelétrico; Peltier

1 INTRODUCTION

The microbial population is a highly relevant factor in indoor air pollution, comprising hundreds of fungal and bacterial species. Among these, filamentous fungi (mold) deserve particular attention, as they thrive in the presence of moisture, enabling their growth and proliferation in indoor environments (Mendell et al., 2009). Damp indoor settings typically host a wide variety of these species due to favorable temperature and humidity conditions. Fungi are frequently found in areas with high humidity, such as damp walls, kitchens, and structures surrounding openings like windows (Mendell et al., 2009).

In this context, relative humidity plays a significant role in respiratory health and may be associated with the exacerbation of conditions such as asthma, respiratory tract infections, coughing, wheezing, dyspnea, and other respiratory complications (Mendell et al., 2009).

Condensation is often an imperceptible phenomenon on surfaces such as walls, books, and cabinets, which promotes mold growth. To survive, mold extracts nutrients from the organic matter present on these surfaces, leading to their deterioration (Galvin, 2010). Exposure to mold may be associated with the development of respiratory illnesses.

Thus, the use of dehumidifiers becomes a viable alternative not only for reducing air humidity but also for obtaining water in regions with climatic instability (Henker et al., 2014). In this context, thermoelectric dehumidifiers based on the Peltier effect stand out as an advantageous solution due to their lightweight design, compact size, silent operation, and lower environmental impact (Henker et al., 2014).

Therefore, the objective of the present study is to analyze a thermoelectric dehumidifier prototype by conducting temperature measurements and mathematically modeling the system, in order to propose the necessary improvements to make it competitive with existing devices on the market.

2 LITERATURE REVIEW

The Peltier effect was first observed in 1834 by Jean Charles Athanase Peltier, who discovered thermoelectric effects after introducing small external electrical currents into a bismuth/antimony thermocouple. The experiments demonstrated that when a small electric current passes through the junction of two different metals in one direction, the junction cools down by absorbing heat energy from the surrounding environment. When the direction of the current is reversed, the junction heats up, transferring heat to the medium in which it is located (Carvalho & Cachoeira, 2016).

A thermoelectric air dehumidifier can be constructed using Peltier-effect modules to generate a temperature difference between the two sides of the semiconductor element. When an electric current is applied to the module's terminals, one side heats up while the other cools down. As the temperature of the surface exposed to ambient air decreases, the relative humidity increases until it reaches saturation, leading to the condensation of water vapor present in the air, thereby reducing the absolute humidity in the surrounding environment. Heat sinks are also required to prevent the generated heat from being absorbed by the Peltier modules, which would otherwise reduce their efficiency and lifespan (Carvalho & Cachoeira, 2016; Vián et al.,2002; Yao et al.,2017).

Alternative dehumidification solutions can be found in both academic literature and commercial markets. These systems operate on the same basic principle as the dehumidifier studied in the present work, but differ in acquisition cost, energy consumption, size, efficiency, and assembly. The prototype presented features a simplified assembly, with a similar production cost, but higher energy consumption (R$0.248 over six hours) and a water production rate of 1 g per hour, resulting in 24.15 g/R$ over six hours of operation. In comparison, the prototype described in (Henker et al., 2014), although designed for a different purpose, has larger dimensions, higher production cost, and significantly greater energy consumption (R$81.96 over six hours), producing 2.6 liters of water per hour, equivalent to 0.031 L/R$ over six hours.

More robust devices, such as the one presented in (Vián et al., 2002), utilize computational optimization of the Peltier module and fan voltage in response to ambient humidity and temperature. This approach yielded an experimental water production rate of 0.040 L per hour at a cost of R$0.248 over six hours, or 0.967 L/R$ for a 100 W dehumidifier.

3 ANALYZED DEHUMIDIFIER

The air dehumidifier prototype used in this study, shown in Figure 1, is built with a steel sheet structure in which a Peltier module was embedded.

Figure 1 – Side and Top View of the Analyzed Dehumidifier
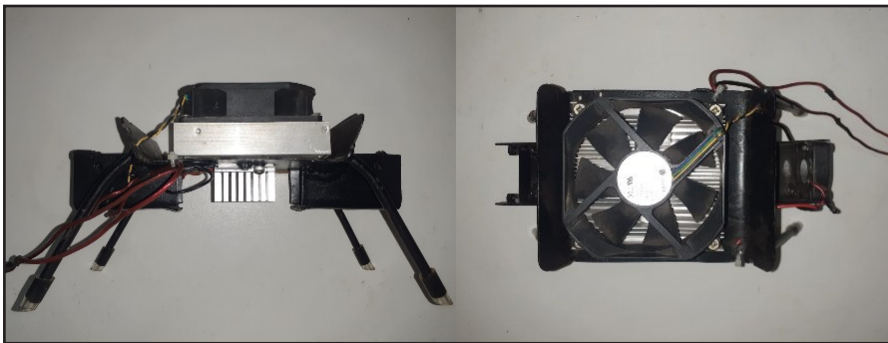
Source: Authors' private collection (11, 2024)

To cool the hot side and condense the water particles from the humid air on the cold side, two finned heat sinks were used one for each surface of the Peltier module. The upper heat sink has dimensions of 80×80 mm and is equipped with an 80 mm fan to remove hot air. The lower heat sink, measuring 40×40 mm, has a 40 mm fan installed parallel to its horizontal direction, which is used to promote forced convection in the system. A 0.5 mm layer of Cooler Master® thermal paste was applied between the heat sinks and the surfaces of the Peltier module, providing a contact thermal resistance of 0.0625 K/W (Cooler Master, 2024).

Table (1) presents the model and technical information of the Peltier module used in the analyzed system.

Table 1 – Specifications of the Peltier Module

Model	TEC1-12706
Seebeck coefficient (α)	53e-3 V/K
Electrical resistance (R)	2,1 Ω
Thermal conductivity (Kt)	1,95 K/W

Source: Kubov, Dymytrov & Kubova (2016)

4 MEASUREMENTS

The methodology of this study comprises two main stages. Initially, experimental measurements of the process variables, temperature and mass flow rate, were carried out following the protocol described in this section. Subsequently, a mathematical model was developed to represent the behavior of the system under study, and the model was validated by comparing the analytical results with the experimental data.

Temperature measurements of the system were conducted in an enclosed environment, where the ambient temperature was 32°C and the dew point was 21°C, at approximately 4:00 p.m. The prototype was tested under a 31 W power condition. During the experiment, after a 15-minute stabilization period, the temperatures at the cold and hot sides were measured using a thermal imaging camera (Flir brand). The system was powered by a supply providing voltage to both the thermoelectric module and the cooling fan. The measurement results for the condition under forced convection are presented in Table (2).

Table 2 – Temperature Measurements for the Forced Convection System

Power	31 W
Voltage	10,0 V
Current	3,1 A
Hot side temperature	28,6$^{\mathrm{o}}$C
Cold side temperature	7,1$^{\mathrm{o}}$C

Source: Authorship (2025)

After the stabilization period, the temperatures shown in Table (2) were measured using a thermal imaging camera, with the corresponding thermal image shown in Figure (2).

Figure 2 –Thermal image under the 31 W condition
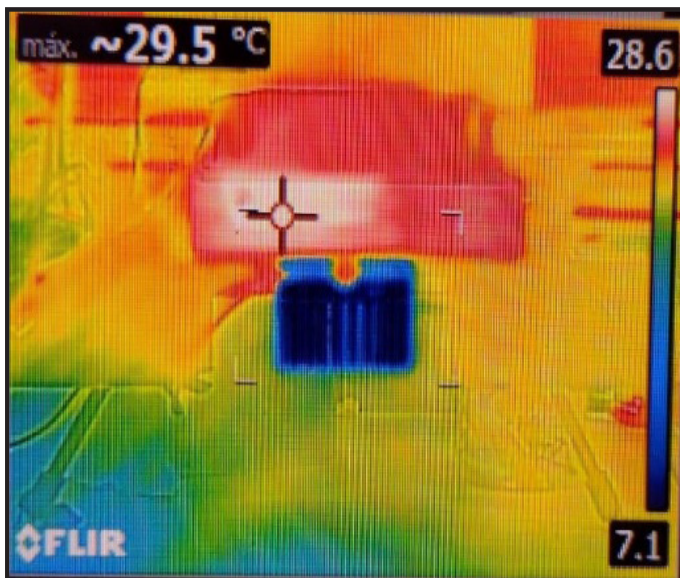
Source: Authors' private collection (11, 2024)

Figure (2) includes a temperature scale on its right side, serving as a reference for the temperature distribution across the prototype. In the upper left corner, the image displays the maximum temperature, corresponding to the region indicated by the reference point.

It is also important to note that thermal cameras measure an object's temperature based on its emissivity in the infrared spectrum, without requiring physical contact. For the tested condition, the emissivity was set to 0.95, a typical value for opaque surfaces. However, this parameter may introduce uncertainties in the measurements, as it does not necessarily match the actual emissivity of the material being measured.

For the water extraction measurements, the dehumidifier operated for a period of 6 hours. In addition to the amount of water collected, the energy consumption during operation was also determined. Table (3) presents the meteorological conditions during the measurements and the mass flow rate of the extracted water.

Table 3 – Extracted Water Mass Flow Rate and Meteorological Conditions During the Measurement

Power	31 W
Voltage	10,0 V
Current	3,1 A
Hot side temperature	22°C
Relative Humidity	90%
Initial Ambient Temperature	26,4°C
Final Ambient Temperature	26,9°C
Produced Water Mass	23 g
Mass Flow Rate	3,833 g/h

Source: Authorship (2025)

Dew point temperature and relative humidity data for the test location were obtained from the AccuWeather® meteorological platform. Ambient temperature measurements were performed using a Fratelli® digital thermometer with a resolution of 0.1°C, while the mass of water produced was measured using an SF 400 digital kitchen scale with a resolution of 1 g.

The operating cost of the device can also be calculated, based on the electricity tariff provided by the utility company RGE in the city of Cachoeira do Sul, RS, Brazil. These data are presented in Table (4).

Table 4 – Electricity Tariff in the City of Cachoeira do Sul, RS, Brazil

Operation	Tariff
System Usage	0,5144 R$/kWh
System Availability	0,348 R$/kWh
Total	0,8624 R$/kWh

Source: RGE (2024)

Thus, with the total tariff presented in Table (4), the power applied to the dehumidifier, and the operation time, it is possible to determine the cost of operation of the system presented in Table (3) as 0.155 R$/gram of water.

When considering industrial dehumidifiers, their performance is measured in volume per unit of time. Assuming the specific mass of water is approximately 1 g/ml the extration rate is 91.992 ml/day. Thus, a comparison between the analyzed prototype and commercially available dehumidifiers can be made. In this way, Table (5) presents information on two dehumidifiers available in the retail market.

Table 5 – Commercial Dehumidifiers

Model	Britânia BDE01	Tubrax Antimofo 500ml	Prototype Analyzed
Power	23.0 W	22.5 W	31.0 W
Performance	300 ml/day	300 ml/day	92 ml/day
Cost	R$ 249.00	R$ 191.90	R$ 131.50

Source: Authorship (2025)

Through this comparison, it is clear that commercial dehumidifiers have superior efficiency. However, it is important to emphasize that the manufacturing cost of the tested model is lower than the others. Furthermore, regarding the measurements, there are errors associated with the values measured on the prototype. Therefore, the development of a mathematical model for the analyzed device becomes essential, as it allows for the identification of areas that need improvement in order to enhance the device's competitiveness compared to those commercially available.

5 MATHEMATICAL MODELING

In order to understand the presented system and propose effective solutions for improving its performance, the development of a mathematical model representing the physical phenomena involved in the device's operations is necessary. This model allows for a quantitative analysis of its behavior and the identification of areas that need improvement.

5.1 Mass Balance

For the subsequent analyses, the control volume considered includes only the region of the Peltier module and the finned surface attached to its cold face, as shown in Figure (3).

Figure 3 – Graphical Representation of the Analyzed Control Volume
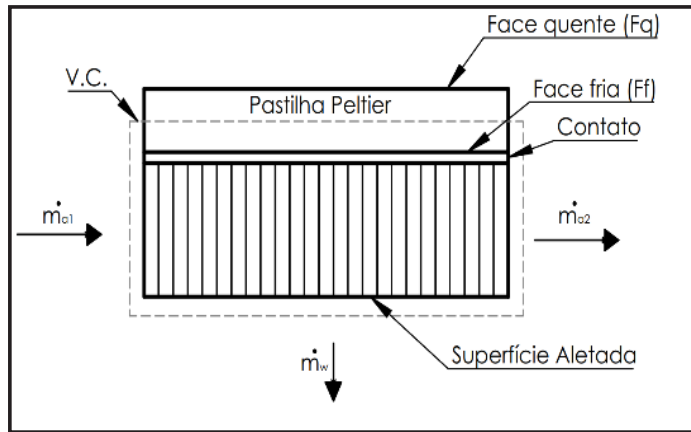
Source: Authors (2025)

Considering the control volume illustrated in Figure (3), where humid air flow occurs, the principle of mass conservation ensures that the mass flow rate of dry air (m_a) remains constant throughout the process. However, since the flow occurs over a cold finned surface, where the temperature is lower than the dew point, condensation of a portion of the water vapor in the air takes place. Thus, the mass flow rate of water can be determined using Equation (1) (Moram et al., 2014).

$$\dot{m}_w = \dot{m}_a \left(\omega_e - \omega_s \right) \tag{1}$$

Where:
m_w represents the mass flow rate of water exiting the control volume;
m_s the mass flow rate of air;
ω_i the specific humidity (kg_water/kg_air) of the flow at the inlet and outlet.

Assuming that the inlet air temperature of the control volume is equal to the ambient temperature (T_∞) and the outlet temperature is equal to the average temperature of the finned surface (T_s), the heat removal rate can be expressed by Equation (2) (Moram et al., 2014).

$$Q_F = \dot{m}_a \cdot (Cp_e \cdot T_\infty - Cp_s \cdot T_s) \tag{2}$$

Where:

Q_f is the heat extraction rate;

C_{pi} are the specific heat capacities at constant pressure for dry air, evaluated at the inlet and outlet temperatures, respectively.

By applying Equation (1) to (2), the heat removal rate can be expressed as a function of the mass flow rate of condensed water, resulting in Equation (3).

$$Q_F = \frac{\dot{m}_w}{(\omega_e - \omega_s)} \cdot (Cp_e \cdot T_\infty - Cp_s \cdot T_s) \tag{3}$$

5.2 Thermal Resistance Modeling

For the subsequent analyses, the control volume considered includes only the region of the Peltier module and the finned surface attached to its cold face, as shown in Figure (3).

The heat removal rate of the Peltier module can also be determined using the thermal resistance method. To find the equivalent thermal resistance of the finned surface, the method described by Teerststra et al. (1999) for a heat sink under forced convection can be applied, with dimensions shown in Figure (4), as presented in Equations (4) to (13).

Figure 4 – Heat Sink Dimensions
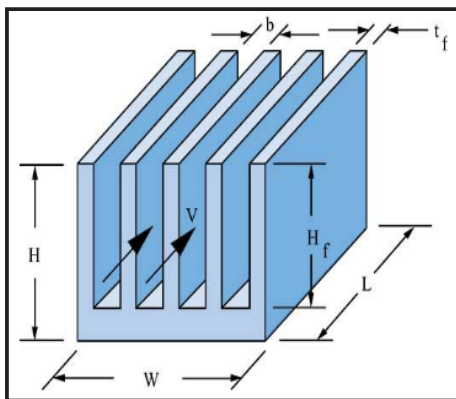
Source: Teerststra *et al.* (1999)

Equation (4) presents the average velocity between the fins (Teerststra et al., 1999).

$$V = \frac{Q}{N_{aletas} \cdot b \cdot H_f}$$
(4)

Where:
Q represents the volumetric air flow rate;
N_{aletas} is the number of fins;
b is the spacing between them;
Hf is their height.

Equation (5) presents the modified expression for the Reynolds number in the channels between the fins (Teerststra et al., 1999).

$$Re = \frac{\rho \cdot V \cdot b^2}{\mu \cdot L}$$
(5)

Where:
ρ is the air density;
μ is its absolute viscosity;
L is the length of the heat sink.

Equation (6) presents the expression for calculating the average Nusselt number for the heat sink (Teerststra et al., 1999).

$$Nu = ((\frac{Re \cdot Pr}{2})^{-3} + (0,664 \cdot \sqrt{Re} \cdot Pr^{0,33} \cdot \sqrt{1 + \frac{3,65}{\sqrt{Re}}})^{-3})^{-0,33}$$
(6)

Thus, the average convective heat transfer coefficient for the heat sink is determined by Equation (7) (Moram et al., 2014).

$$\bar{h} = \frac{Nu \cdot k_f}{b}$$
(7)

Where:
k_f represents the thermal conductivity of the fluid.

Thus, the total thermal resistance, Equation (8), of the heat sink can be expressed as a function of the convection resistance, conduction resistance at its base, and contact resistance with the Peltier module.

$$R_{total} = [\bar{h} \cdot (A_{base} + N_{aletas} \cdot \eta_{aleta} \cdot A_{aleta})]^{-1} + \frac{H - H_f}{k_{base} \cdot W \cdot L} + R_{contato} \tag{8}$$

Where:
$\bar{h}$ is the average convective heat transfer coefficient;
A_{base} is the base area given by Equation (9);
η_{aleta} represents the efficiency of each fin as given by Equation (10);
A_{aleta} is its surface area determined through Equation (11);
k_{base} represents the thermal conductivity of the base material;

$R_{contato}$ is the thermal contact resistance between the heat sink and the Peltier module.

$$A_{base} = (N_{aletas} - 1) \cdot b \cdot L \tag{9}$$

$$\eta_{aleta} = \frac{tanh(m \cdot H_f)}{m \cdot H_f} \quad \text{onde } m = \sqrt{\frac{2 \cdot \bar{h}}{k_{aleta} \cdot t_{aleta}}} \tag{10}$$

$$A_{aleta} = 2 \cdot H_f \cdot L \tag{11}$$

Thus, the heat removal rate generated by the cold surface of the Peltier module can be expressed through Equation (12) (Incropera et al. 2014).

$$T_\infty - T_F = Q_F \cdot R_{total} \tag{12}$$

Where:
T_∞ is the ambient temperature;
T_f is the temperature at the cold face of the Peltier module.

5.3 Energy balance on the Peltier module

The heat removal rate of the Peltier module can also be expressed as a function of the electrical variables applied to the device, such as voltage and current. The equations describing this phenomenon take into account the thermoelectric properties of the

semiconductor material, such as the Seebeck coefficient, which relates the generated electrical potential difference to the temperature difference between the junctions, and the electrical and thermal resistances, which characterize the ohmic and thermal losses in the device. Equation (13) summarizes this relationship (Srivastava et al., 2021).

$$Q_F = \alpha \cdot I \cdot T_F - 0{,}5 \cdot I^2 \cdot R - k_t^{-1} \cdot (T_Q - T_F) \tag{13}$$

Where:
α is the Seebeck coefficient [V/K];
I is the applied electric current;
T_f is the temperature of the cold face;
T_Q is the temperature of the hot face;
R is the electrical resistance;
Kt is the thermal conductivity of the Peltier module.

Equation (14) can be used to correlate the applied electrical power to the module with its temperature difference (Srivastava et al., 2021).

$$P_e = \alpha \cdot I \cdot (T_Q - T_F) + I^2 \cdot R \tag{14}$$

Where:
P_e is the electrical power applied to the module.

5.4 Mathematical model

Equations (13) and (14) are directly dependent on the temperatures of the interfaces of the Peltier module, which complicates validation in complex systems due to temperature measurement errors at such interfaces. Alternatively, the power consumed can be determined experimentally from voltage and current measurements, allowing the elimination of the temperature difference dependence in Equation (13) by applying Equation (14), resulting in Equation (15).

$$Q_F = \alpha \cdot I \cdot T_F - 0{,}5 \cdot I^2 \cdot R - k_t^{-1} \cdot \left(\frac{P_e - I^2 \cdot R}{\alpha \cdot I}\right) \tag{15}$$

However, Equation (15) still presents a dependence on the temperature of the cold face, which can be resolved by applying Equation (12), leading to Equation (16).

$$Q_F = [\alpha \cdot I \cdot T_\infty - 0{,}5 \cdot I^2 \cdot R - k_t^{-1} \cdot (\frac{P_e - I^2 \cdot R}{\alpha \cdot I})] \cdot (1 + \alpha \cdot I \cdot R_{total})^{-1} \tag{16}$$

The mass flow rate of water can be directly related to the heat extraction rate provided by the Peltier module through Equation (3). Thus, a single expression for the water mass flow rate can be obtained and is presented in Equation (17).

$$mi_w = \frac{[\alpha \cdot I \cdot T_\infty - 0{,}5 \cdot I^2 \cdot R - k_t^{-1} \cdot (\frac{P_e - I^2 \cdot R}{\alpha \cdot I})] \cdot (\omega_e - \omega_s)}{(1 + \alpha \cdot I \cdot R_{total}) \cdot (Cp_e \cdot T_\infty - Cp_s \cdot T_s)} \tag{17}$$

Thus, the resulting equation for the mass flow rate of water produced by the dehumidifier accounts only for the properties of the Peltier module used, the meteorological conditions, and the design characteristics of the device.

5.5 Verification of the mathematical model

To verify the validity of the mathematical model presented in Equation (17), the experimental data obtained for the 31 W power configuration, shown in Table (3), were used under the same meteorological conditions for the determination of thermophysical properties.

A code developed in the commercial software Engineering Equation Solver (EES) was used to perform the calculations and determine the required properties. The assumptions adopted for the model are listed below:

•The system operates under steady-state conditions;

•The flow is incompressible, with a Mach number below 0.3 due to low velocities;

•The moist air in the flow is modeled as an ideal gas mixture;

•The pressure is constant throughout the system and equal to atmospheric pressure;

•Heat transfer is assumed to occur unidirectionally between the Peltier module and the heat sink;

•The thermal contact resistance between these surfaces is considered as specified by the thermal paste manufacturer;

•The properties of the Peltier module are assumed to be constant;

•The air temperature at the inlet of the control volume (Figure 3) is assumed to be equal to the ambient temperature ($T_\infty = T_{ambient}$);

•The air temperature at the outlet of the control volume is assumed to be equal to the average temperature of the finned surface T_s;

•The thermophysical properties are determined based on the average temperature between T_∞ and T_s;

•For the verification calculations of the mathematical model, Equation (1) was used to determine the mass flow rate of air passing through the control volume, and Ts was taken as the temperature measured using the thermal camera, as shown in Table (3).

Table (6) presents a comparison between the experimentally and analytically obtained results for the mass flow rate of condensed water under the 31 W power condition, as presented in Table (3).

Table 6 – Comparison Between the Analytical Model and the Experimental Data

Parameter	Experimental	Analytical	Deviation
Water Mass Flow Rate	1.065×10^{-6} kg/s	1.273×10^{-6} kg/s	
Heat Extraction Rate	1.45 W	1.74 W	16.3%
Process Efficiency	4.85%	5.8%	

Source: Authorship (2025)

Table (6) demonstrates good agreement between the analytical model and the experimentally obtained data. It can be inferred that the 16.3% divergence stems from a combination of factors, including inherent errors in the experimental measurement process, the assumptions used in developing the model (presented throughout the text and listed above), and the error associated with determining the convective thermal resistance through empirical correlations for the average Nusselt number. Nevertheless, Equation (17) remains valid for assessing potential system improvements.

6 PROPOSED IMPROVEMENTS

Analysis of Equation (17) reveals that without modifying the electrical power supplied to the device, meteorological conditions, or characteristics of the Peltier module, water extraction can be altered by changing the total thermal resistance. Specifically, reducing this resistance results in an increased mass flow rate of water.

By examining Equations (5) through (8), two primary modifications can be identified to enhance system efficiency: increasing the Reynolds number and modifying the heat sink geometry. However, due to the numerous geometric parameters of the heat sink involved in calculating the produced water mass flow rate, a more comprehensive and complex analysis would be required to determine the optimal heat sink parameters. Such an analysis falls beyond the scope of this work.

Therefore, for the studied device, the key improvement to increase water extraction is adjusting the Reynolds number. Figure (6) illustrates the relationship between this parameter and the water mass flow rate.

Figure 5 – Relationship Between the Extracted Water Mass Flow Rate and the Reynolds Number
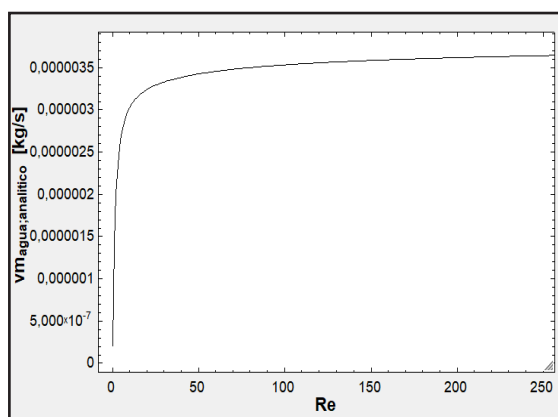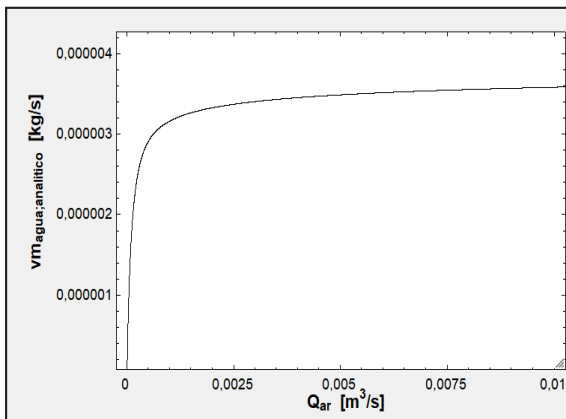

Source: Authors (2025)

Thus, it is evident that the analyzed system is not in its optimal configuration, as the obtained Reynolds number was 0.92, while the analytical model suggests values greater than 50 as ideal, as shown in Figure (6).

By maintaining the geometric parameters of the heat sink used, the water extraction can then be evaluated as a function of the volumetric air flow rate through the system, as presented in Figure (7).

Figure 6 – Relationship Between the Extracted Water Mass Flow Rate and the Air Volumetric Flow Rate

Source: Authors (2025)

The analyzed device exhibits an air volumetric flow rate of 6.15×10^{-5} m³/s. As shown in Figure (7), this represents a flow rate 40 times lower than the minimum adequate value of 2.5×10^{-3} m³/s. Therefore, replacing the current cooling fan with one capable of achieving this minimum flow rate could potentially triple the extracted water mass flow rate.

7 CONCLUSIONS

Through the comparative analysis between the analytical and experimental models, it is possible to validate the reliability of the analytical model, which shows discrepancies within the expected error margins for this type of approach, given the assumptions considered. However, when evaluating its feasibility, it was found that the current system exhibits low efficiency, resulting from an inadequate design of the geometric parameters and the minimum air flow rate required to ensure a meaningful and viable water production. Therefore, in order to maximize the project's efficiency and feasibility, it is essential to implement the modifications outlined in this article.

REFERENCES

Britânia. (s.d.). Desumidificador Britânia 1,1L 7 Cores de Iluminação BDE01. https://www.britania.com.br/desumidificador-bde01-touch-biv-065503023/p?idsku=22362&gad_source=4&gclid=CjwKCAiA6aW6BhBqEiwA6KzDc3UhLssFFv_0HanV3xipFRHZzzXVO8cqHrmxeeSeSh3QsCqVrQBElRoCmmEQAvD_BwE.

Carvalho, L., Raphael, R., & Cachoeira, T. (2016). *Análise de sistema de obtenção de água através de desumidificação do ar com uso de célula peltier*. CEFET, Rio de Janeiro. https://www.cefet-rj.br/attachments/article/2943/An%C3%A1lise%20de%20sistema%20de%20obten%C3%A7%C3%A3o%20de%20%C3%A1gua%20atrav%C3%A9s%20de%20desumidifica%C3%A7%C3%A3o%20do%20ar%20com%20uso%20de%20c%C3%A9lula%20Pelti.pdf.

Cooler Master. (s.d.). *High Performace Thermal Paste*. https://www.coolermaster.com/en-global/products/high-performance-thermal-paste/?tab=tech_spec.

Galvin, R. (2010). Solving mould and condensation problems: A dehumidifier trial in a suburban house in Britain. *Energy and Buildings*, 42(11), 2118–2123.

Henker, E., et al. (2014). *Água potável com desumidificação do ar e energia solar: adaptação ao stress hídrico no RS*. 19(3), 345–352.

Incropera, F. P., & DeWitt D. P. (2014). *Fundamentos da Transferência de Calor e de Massa (7a ed.)*. LTC Editora.

Kubov, V. I., Dymytrov Y. Y., & Kubova, R. N. (2016). LTspice-model of Thermoelectric Peltier-Seebeck Element. In *2016 IEEE 36th International Conference on Electronics and Nanotechnology (ELNANO)*, 47-51.

Mendell, M. J. et al. (2009). Health effects associated with dampness and mould. In Organização Mundial da Saúde. *WHO guidelines for indoor air quality: dampness and mould*.

Moram, M. J., Shapiro, H. N., Boettner, D. D., & Bailey, M. B. (2014). *Princípios de Termodinâmica para Engenharia*, (7a ed.). LTC Editora.

Srivastava, R. S., et al. (2021). Development and applications of thermoelectric based dehumidifiers. *Energy and Buildings*, 252, 111-446.

Teertstra, P., Yovanovich, M. M., & Culham, J. R. (1999) Analytical forced convection modeling of plate fin heat sinks. *Proceedings of 15th IEEE Semi-Therm Symposium*, 34-41.

Tubrax. (s.d.). *Mini Desumidificador Elétrico 127-220v Antimofo 500ml Tubrax*. Leroy Merlin. https://www.leroymerlin.com.br/mini-desumidificador-eletrico-127-220v-antimofo-500ml-tubrax_1567811425?region=outros&srsltid=AfmBOory2ezmkFuJwaS-_X84Rqdx7V4WY3x4aT-R8G1veUeBJ-ZBiR8XlH8#descricao-do-produto.

Vián, J. G., Astrain, D., & Domínguez, M. (2002) Numerical modelling and a design of a thermoelectric dehumidifier. *Applied thermal engineering*, 22(4), 407–422. https://doi.org/10.1016/S1359-4311(01)00102-8

Yao, Y., et al. (2017). Optimization design and experimental study of thermoelectric dehumidifier. *Applied Thermal Engineering*, 123, 820–829.

Authorship contributions

1 – Mathias Verdum de Almeida

Mechanical Engineering Academic at Universidade Federal de Santa Maria (UFSM) – Cachoeira do Sul.
https://orcid.org/0009-0002-5371-9441 • mathias.verdum@acad.ufsm.br
Contribution: Writing – original draft, Writing – review & editing

2 – Arthur Sandri Lunkes

Mechanical Engineering Academic at Universidade Federal de Santa Maria (UFSM) – Cachoeira do Sul.
https://orcid.org/0009-0005-7750-8421 • arthur.lunkes@acad.ufsm.br
Contribution: Writing – original draft, Writing – review & editing

3 – Juan Augusto Mayer Copetti

Mechanical Engineering Academic at Universidade Federal de Santa Maria (UFSM)– Cachoeira do Sul.
https://orcid.org/0009-0009-8254-0724 • juan.copetti@acad.ufsm.br
Contribution: Writing – original draft, Writing – review & editing

4 – Matheus Fritz Warol Porto Rodrigues

Mechanical Engineering Academic at Universidade Federal de Santa Maria (UFSM) – Cachoeira do Sul.
https://orcid.org/0009-0000-1758-5306 • matheus.porto@acad.ufsm.br
Contribution: Writing – original draft, Writing – review & editing

5 – Maximiliano Silveira de Souza

Mechanical Engineering Academic at Universidade Federal de Santa Maria (UFSM) – Cachoeira do Sul.
https://orcid.org/0009-0000-5236-0196 • maximiliano.silveira@acad.ufsm.br
Contribution: Writing – original draft, Writing – review & editing

6 – Cristiano Frandalozo Maidana

PhD in Mechanical Engineering and Professor of the Mechanical Engineering Course at Universidade Federal de Santa Maria (UFSM) – Cachoeira do Sul.
https://orcid.org/0000-0003-3137-6177 • cristiano.maidana@ufsm.br
Contribution: Writing – review & editing

7 – Charles Rech

PhD in Mechanical Engineering and Professor of the Mechanical Engineering Course at Universidade Federal de Santa Maria (UFSM) – Cachoeira do Sul.
https://orcid.org/0000-0001-8523-6300 • charles.rech@ufsm.br
Contribution: Writing – review & editing

8 – André Francisco Caldeira

PhD in Automation and Systems and Professor of the Mechanical Engineering Course at Universidade Federal de Santa Maria (UFSM) – Cachoeira do Sul.
https://orcid.org/0000-0002-4939-2709 • andre.caldeira@ufsm.br
Contribution: Writing – review & editing

9 – Simone Ferigolo Venturini

PhD in Production Engineering at Universidade Federal de Santa Maria (UFSM).
https://orcid.org/0000-0002-9439-0008 • simone.venturini@gmail.com
Contribution: Writing – review & editing

10 – Carmen Brum Rosa

Professor of the Postgraduate Program in Production Engineering (PPGEP) at Universidade Federal de Santa Maria.
https://orcid.org/0000-0002-0173-081X • carmen.b.rosa@ufsm.br
Contribution: Writing – review & editing

How to quote this article

Almeida, M. V. de ., Lunkes, A. S., Copetti, J. A. M., Rodrigues, M. F. W. P., Souza, M. S. de, Maidana, C. F., Rech, C., Caldeira, A. F., Venturini, S. F., & Rosa, C. B. (2025). Análise de um Desumidificador Termoelétrico. *Ciência e Natura*, Santa Maria, v. 47, spe. 4. DOI 10.5902/217946092122. Disponível em: https://doi.org/10.5902/217946092122.